Exploiting Spin Fluctuations for Enhanced Pure Spin Current

Po-Hsun Wu,[1,2] Danru Qu,[3,*] Yen-Chang Tu,[1] Yin-Ze Lin,[1] C. L. Chien,[1,2,†] and Ssu-Yen Huang[1,‡]
[1]Department of Physics, National Taiwan University, Taipei 10617, Taiwan
[2]Department of Physics and Astronomy, Johns Hopkins University, Baltimore, Maryland 21218, USA
[3]Center for Condensed Matter Sciences, National Taiwan University, Taipei 10617, Taiwan

(Received 13 September 2021; revised 13 February 2022; accepted 9 May 2022; published 1 June 2022)

We demonstrate the interplay of pure spin current, spin-polarized current, and spin fluctuation in 3d Ni_xCu_{1-x}. By tuning the compositions of the Ni_xCu_{1-x} alloys, we separate the effects due to the pure spin current and spin-polarized current. By exploiting the interaction of spin current with spin fluctuation in suitable Ni-Cu alloys, we obtain an unprecedentedly high spin Hall angle of 46%, about 5 times larger than that in Pt, at room temperature. Furthermore, we show that spin-dependent thermal transport via anomalous Nernst effect can serve as a sensitive magnetometer to electrically probe the magnetic phase transitions in thin films with in-plane anisotropy. The enhancement of spin Hall angle by exploiting spin current fluctuation via composition control makes 3d magnets functional materials in charge-to-spin conversion for spintronic application.

DOI: 10.1103/PhysRevLett.128.227203

Spintronics has evolved from exploiting spin-polarized current phenomena [e.g., giant magnetoresistance [1,2] and spin transfer torque [3,4]] in ferromagnetic materials to pure spin-current phenomena (e.g., spin Hall effect (SHE) [5–7] and spin-orbit torque (SOT) [8–10]) in materials with strong spin-orbit coupling (SOC). A pure spin current has the unique attribute of efficiently delivering spin angular momentum with minimum charge carriers in metals and no charge carriers in insulators. A large variety of materials have been explored as pure spin current materials, including semiconductors [11,12], transition metals and their alloys [13–15], topological insulators, semimetals, transition metal dichalcogenides [16–19], and more. For the transition metals, the values of spin Hall angles (θ_{SH}) are dictated by the band structures and inherent to the specific metals. While some 3d metals (e.g., Cu) have weak SOC and $\theta_{SH} \approx 0$, others, including ferromagnetic (FM) and antiferromagnetic (AFM) metals (e.g., Ni and Cr), exhibit large inverse spin Hall effect (ISHE) and substantial θ_{SH} [20–23]. Indeed, the 3d metals have provided new avenues and functionalities for pure spin-current explorations, including spin-to-charge conversion, magnetization-dependent spin Hall effect, and spin-orbit torque magnetization switching [20,24–26].

Unlike the 5d metals, which are usually nonmagnetic, the 3d metals are often ferromagnetic (e.g., Fe, Ni, Co) or antiferromagnetic (e.g., Mn, Cr), where both pure spin-current effects and spin-polarized current effects coexist, which must be delineated albeit challenging. For the 3d magnetic materials, the enhancement of spin current at the critical temperatures due to spin fluctuation is one of the most intriguing spin-current phenomena, which has been intensely studied in AFMs [27–31], but less so in FMs [32,33], where the physical phenomena caused by spin-polarized current and pure spin current are better established. The well-known 3d magnets of Fe, Co, Ni, and Py (permalloy = $Ni_{81}Fe_{19}$) have very high Curie temperatures (T_C), with the accessible temperatures limited to only $T < T_C$. Thus, it is difficult to separate effects due to spin-polarized current and pure spin current, let alone explore the promising role of spin fluctuations near or above T_C. It is essential to select suitable 3d FM materials with tailored T_C, where effects due to spin-polarized current and pure spin current can be cleanly delineated, separated, and even possibly exploited. Several pioneering works, including the weakly ferromagnetic NiPd alloy by the nonlocal spin injection technique [32] and ferromagnetic FePt alloy by the harmonic transverse Hall measurement [33], study the interplay among spin current, spin polarization, and spin fluctuation. But in these cases, the 4d and 5d heavy metals serve as the host materials, and their contribution to the SHE cannot be ignored. To avoid the complication from heavy metals, we have selected the Ni-Cu alloys, where the magnetic ordering temperature T_C can be tuned over a wide range through varying the Ni content [34,35].

Besides the selection of suitable 3d FM materials, it is also important to choose suitable measurement techniques. There are various ways to generate spin-polarized current and pure spin current, including electrical current (e.g., anomalous Hall [36], spin Hall, and multiterminal nonlocal method [37]), thermal gradient (e.g., anomalous Nernst [38], spin Seebeck [39]), and ferromagnetic resonance (e.g., spin pumping [40]). While the charge current distribution in the electrical generation of the spin current is nontrivial, the ferromagnetic resonance (FMR) may

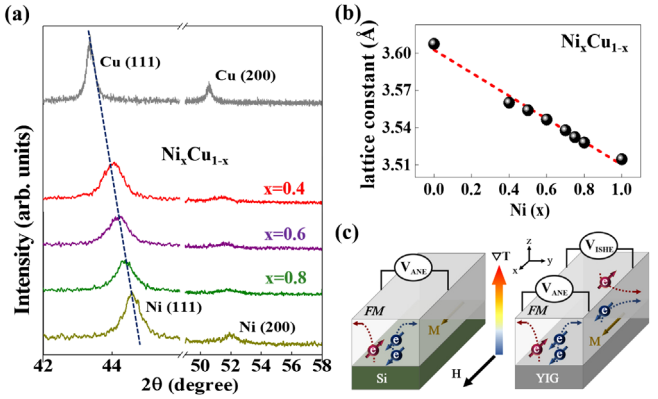

FIG. 1. (a) X-ray diffraction pattern of the 200-nm-thick Ni_xCu_{1-x} ($0 < x < 1.0$) with different compositions. (b) The composition dependence of lattice constant (a) for Ni_xCu_{1-x}. (c) Schematics of anomalous Nernst effect (ANE) in a ferromagnetic metal (FM) and inverse spin Hall effect (ISHE) and ANE in FM/YIG under a temperature gradient.

inadvertently include other contributions, especially thermal effects due to the high FMR heating [41,42]. Among these approaches, the longitudinal thermal spin injection method through ferromagnetic insulator has the simplest injection scheme and fewer complications.

As shown in Fig. 1(c), for a FM with in-plane magnetization along the x direction, a temperature gradient (∇T) in the out-of-plane (z) direction injects a charge current in the z direction. The SOC in the FM causes unequal amount of spin-up and spin-down electrons to deflect laterally in opposite directions, resulting in a spin-polarized current, contributing to the anomalous Nernst effect (ANE) electric field in the y direction,

$$\boldsymbol{E}_{\mathrm{ANE}} = -Q_S 4\pi \boldsymbol{M} \times \nabla T, \tag{1}$$

and detected as an ANE voltage, where Q_s is the ANE coefficient [38]. The ANE readily measures the hysteresis loop and T_C in thin FM films with only a few nanometer thick. It can function as a sensitive magnetometer for probing the in-plane magnetization of FM with in-plane magnetization, in a manner similar to that of anomalous Hall effect as a sensitive magnetometer for probing the perpendicular magnetization of FM with perpendicular magnetization. In addition, the heat current perpendicular to the plane also captures the interface or multilayer contributions, similar to the current-perpendicular-to-plane measurement but without the challenge of nanoscale device fabrication.

In the longitudinal Spin Seebeck effect (SSE) scheme, a vertical temperature gradient in yttrium iron garnet (YIG) injects a pure spin current $\boldsymbol{j}_S$ into the attached metallic layer in the z direction. With spin index $\boldsymbol{\sigma}$ in the x direction, the SOC causes both spin-up and spin-down electrons to deflect laterally to the same side, contributing to the ISHE electric field in the y direction,

$$\boldsymbol{E}_{\mathrm{ISHE}} \propto \boldsymbol{\sigma} \times \nabla T, \tag{2}$$

and is detected as an ISHE voltage. For a FM metal, with magnetization in the x direction, the electrical fields due to ANE and ISHE are both in the y direction, thus their voltages are additive.

In our Letter, by using the thermal spin injection method from YIG, we report the interplay between the ISHE of the pure spin current and the ANE of the spin-polarized current in Ni-Cu alloys. We observe strong pure spin-current effects in both the FM states and the paramagnetic (PM) states of the Ni-Cu alloys, with and without the spin-polarized current effects, respectively. We exploit spin fluctuation, which is unique to magnetic metals, to greatly enhance spin-to-charge conversion. We obtain spin Hall angles θ_{SH} much larger than those of Pt, Ta, and W. We further show that ANE can function as a sensitive magnetometer to electrically probe the T_C of very thin FM films with only a few nanometer thickness.

We use magnetron cosputtering from Ni and Cu sources to fabricate thin films of Ni_xCu_{1-x}. The composition is controlled by the deposition rates, and subsequently determined by electron probe x-ray microanalyzer. We deposit Ni_xCu_{1-x} thin films on polycrystalline YIG and thermally oxidized Si substrates for measurements with and without pure spin current, respectively. We use x-ray reflectometry and atomic force microscope to measure film thickness and surface roughness, x-ray diffraction (XRD) to measure crystal structures and film orientations, and magnetometers to measure the magnetic properties of Ni_xCu_{1-x} thin films. For spin-dependent transport measurements, we pattern the Ni_xCu_{1-x}, which are capped by 2-nm Al, into Hall bar structures with widths of 200 μm by photolithography.

The XRD patterns of the 200-nm-thick Ni_xCu_{1-x} indicate these alloys are all face centered cubic (fcc) structures with (111) texture, as shown in Fig. 1(a). With increasing Ni content, the (111) peak progressively shifts to higher diffraction angles because of the smaller lattice constant of 0.351 nm of Ni than that of 0.361 nm of Cu. The fcc lattice parameter (a) depends linearly on the Ni content, a manifestation of Vegard's law [43,44], as shown in Fig. 1(b). We use a SQUID magnetometer with high sensitivity to measure the small magnetization ($\sim 10^{-5}$ emu) and the magnetic ordering temperature of the 5-nm Ni_xCu_{1-x} thin film, where a small external in-plane magnetic field of 10 Oe is applied during the measurement. The temperature-dependent magnetization measurement for $Ni_{75}Cu_{25}(5)/Si$ (the number in parentheses is the thickness in nanometers) is shown in Fig. 2(a), which reveals a T_C of 255 K. The hysteresis loops at $T < T_C$ are shown in the Supplemental Material [45].

We use the longitudinal thermal injection in the out-of-plane direction to study the interplay among ISHE, ANE, and spin fluctuations [26]. We use a constant heat flux (Q/A) [46] with a constant heat (Q) and the same sample cross sections (A) to ensure the same temperature gradient

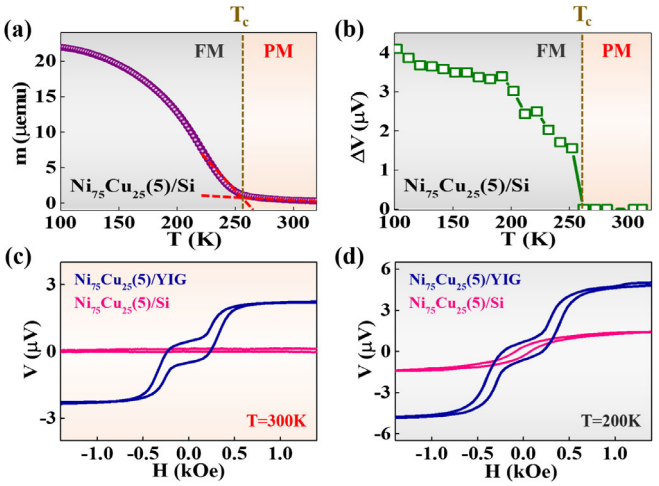

FIG. 2. Temperature-dependent (a) magnetization and (b) anomalous Nernst effect of $Ni_{75}Cu_{25}(5)/Si$. The spin-dependent thermal voltage as a function of magnetic field (H) is measured in $Ni_{75}Cu_{25}(5)/Si$ (blue) and $Ni_{75}Cu_{25}(5)/YIG$ (pink) at (c) 300 K and (d) 200 K, above and below its T_C, respectively.

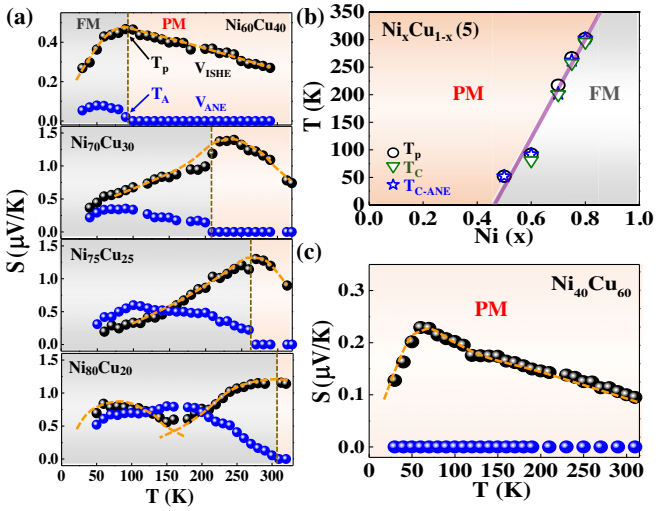

FIG. 3. (a) Temperature-dependent ANE (blue) and ISHE (black) voltage for Ni_xCu_{1-x} with $x = 0.5$, 0.6, 0.7, 0.75, and 0.8. (b) Values of T_p (black circle), T_A (blue star), and T_C (green triangle) as a function of Ni_xCu_{1-x} compositions. (c) Temperature-dependent ANE (blue) and ISHE (black) voltage of $Ni_{40}Cu_{60}$.

(∇T) across the NiCu thin films on various substrates, thus the same ANE voltages (see Supplemental Material [45]). As shown in Figs. 2(c) and 2(d), the ANE voltage in $Ni_{75}Cu_{25}(5)/Si$, while it is sizable at 200 K, vanishes at 300 K. The ANE voltage in fact vanishes abruptly at T_C of 255 K, as shown in Fig. 2(b). The ANE loop at 200 K as shown in Fig. 2(d) reveals the coercivity of $Ni_{75}Cu_{25}(5)$. When $Ni_{75}Cu_{25}(5)/YIG$ is subjected to an out-of-plane temperature gradient of 20 K/mm, in addition to the ANE, there is also ISHE voltage in $Ni_{75}Cu_{25}(5)$ due to the pure spin-current injection from YIG via the SSE. As shown in Figs. 2(c) and 2(d), one observes voltage in $Ni_{75}Cu_{25}(5)/YIG$ not only at 200 K but also at 300 K above T_C, where there is only pure spin current. The plateaus in the low field region of the ISHE voltages are due to demagnetizing factor from surface magnetization of YIG [54]. The lateral voltages measured due to ANE and ISHE shown in Fig. 2 saturate at large $\pm H$ fields. These extremal values define the value of ΔV. In $Ni_{75}Cu_{25}(5)/Si$, one observes only $\Delta V = V_{ANE} = 2.6\ \mu V$ at 200 K and 0 μV at 300 K. However, in $Ni_{75}Cu_{25}(5)/YIG$, under a similar temperature gradient, one observes $\Delta V = \Delta V_{ISHE} = 5\ \mu V$ at 300 K when $Ni_{75}Cu_{25}(5)$ is paramagnetic with $\Delta V_{ANE} = 0$. Importantly, one observes an even larger $\Delta V = \Delta V_{ISHE} + \Delta V_{ANE} = 9.5\ \mu V$ at 200 K that contains both the ANE and the ISHE contributions. These results provide clear evidence that FMs exhibit substantial spin-to-charge conversion in the ferromagnetic state as well as in the paramagnetic state.

We display these ISHE and ANE voltages in $S(\mu V/K) = \Delta V/\Delta T$, where ΔT is the temperature difference. We obtain ΔV_{ANE} and ΔV for Ni_xCu_{1-x}/Si and Ni_xCu_{1-x}/YIG, respectively. By subtracting ΔV_{ANE} from ΔV, we obtain ΔV_{ISHE}. Figure 3(a) shows $S(\mu V/K)$ of Ni_xCu_{1-x} as a function of temperature for a range of compositions ($0.4 \le x \le 0.8$). The $S(\mu V/K)$ of Ni_xCu_{1-x}/Si (blue spheres), consisting of only ΔV_{ANE}, reveals a sharp phase transition at $T_{C\text{-}ANE}$, where T_C is determined by ANE, above which Ni_xCu_{1-x} is in the paramagnetic state with no ANE. On the other hand, $S(\mu V/K)$ of Ni_xCu_{1-x}/YIG (black spheres), containing in addition the pure spin-current contribution, is always substantial, both below and even above T_C.

Also prominently displayed is the pure spin-current enhancement due to spin fluctuations, most intensely near T_C, at which $S(\mu V/K)$ is maximal. Above T_C, spin fluctuation decreases with increasing temperature, so is its effect on the enhancement of spin-to-charge conversion. The magnetic ordering temperature of Ni-Cu alloys is shown in Fig. 3(b), where the values of T_C, $T_{C\text{-}ANE}$, and T_P, determined, respectively, by magnetometry, vanishing ANE in Ni-Cu/Si, and maximal $S(\mu V/K)$ in Ni-Cu/YIG, are in good agreement. All three methods can be used to determine the ordering temperatures of FM materials. But the ANE method enjoys the clear advantages of higher sensitivity. It is especially beneficial for thin films since ANE has no contributions from the thick substrate that plagues magnetometry. In Ni_xCu_{1-x}, the ordering temperature decreases linearly with reducing Ni content, and becomes nonmagnetic at about $x = 0.45$. While there is no magnetic ordering and no ANE in $Ni_{40}Cu_{60}/Si$ down to about 20 K, there is substantial $S(\mu V/K)$ at all temperatures in $Ni_{40}Cu_{60}/YIG$, that increases with decreasing temperature, reflecting the incipient magnetic ordering and the presence of spin fluctuation. Below 60 K, $S(\mu V/K)$ decreases sharply toward zero as expected when $T = 0$ K approaches. These

results show clearly that spin fluctuations in Ni-Cu alloys can greatly enhance the already substantial spin-to-charge conversion. On the other hand, the competition between the propagation length of magnon and the concentration of magnon in YIG can also lead to similar nonmonotonic temperature-dependent behavior of $S(\mu V/K)$ (e.g., Pt/YIG), with S peaks at T_m [55]. The peak caused by the magnons in YIG can be well distinguished from the peak caused by spin fluctuation in NiCu when the NiCu ordering temperature is high. As shown in the bottom panel of Fig. 3(a), for $Ni_{80}Cu_{20}$, two separated peaks are observed at about $T_m = 70$ K [49,56] and $T_C = 300$ K. It is worth pointing out that the two separated ISHE peaks in $Ni_{80}Cu_{20}$/YIG caused by magnons in YIG and the magnetic instability in $Ni_{80}Cu_{20}$ reveal a major difference between the magnons generated from SSE and ferromagnetic resonance, where the latter could be strongly coupled to the magnons in the injected metallic FM layers, causing difficulty in the accurate evaluation of the spin current during spin fluctuation [57].

The interplay of the pure spin current and the spin-polarized current can also be apparent at room temperature when one compares the spin-dependent thermal voltages of ANE and ISHE for 5-nm Ni_xCu_{1-x} in a wide range of compositions ($0 \le x \le 1.0$). As shown in Fig. 4(a), the ΔV_{ISHE} (black spheres) measured at 300 K increases with the Ni content until $Ni_{80}Cu_{20}$, beyond which ΔV_{ISHE} decreases with the simultaneous appearance of ΔV_{ANE}, as 5-nm Ni_xCu_{1-x} with $x > 0.8$ is ferromagnetic. Therefore, in the specific case of $Ni_{80}Cu_{20}$, the spin current can be substantially enhanced near room temperature through spin fluctuation at the phase transition.

To quantitatively determine the enhanced spin-to-charge efficiency of $Ni_{80}Cu_{20}$ at room temperature, we conduct thickness-dependent ISHE measurements in $Ni_{80}Cu_{20}$ to evaluate θ_{SH} and spin diffusion length λ_{sf}. The ISHE voltage is expressed as [14,49]

$$\Delta V_{ISHE}(t) = 2CL\nabla T\rho(t)\theta_{SH}\frac{\lambda_{st}}{t}\tanh\left(\frac{t}{2\lambda_{sf}}\right), \quad (3)$$

where $L = 6$ mm is the distance between the voltage terminals, $|\nabla T| = 26$ K/mm is the temperature gradient, C is the spin-current injection coefficient (see Supplemental Material [45]), and $\rho(t)$ is resistivity. From the linear interpolation with $C(\mathrm{Ni}) = 1.55\ \mathrm{A\,m^{-1}\,K^{-1}}$ for Ni and $C(\mathrm{Cu}) = 1.24\ \mathrm{A\,m^{-1}\,K^{-1}}$ for Cu [21], we obtain $C(Ni_{80}Cu_{20}) = 1.5\ \mathrm{A\,m^{-1}\,K^{-1}}$ for $Ni_{80}Cu_{20}$. For nonmagnetic metals (e.g., Pt), $\Delta V_{ISHE}(t)/\rho(t)$ decreases with increasing t in a quasihyperbolic manner. However, $\Delta V_{ISHE}(t)/\rho(t)$ for $Ni_{80}Cu_{20}$ exhibits a discontinuity at $t = 7$ nm due to magnetic phase transition (see Supplemental Material [45]), as shown in Fig. 4(b). Samples of $Ni_{80}Cu_{20}$ with t greater (less) than 7 nm have T_C above (below) 300 K (see Supplemental Material [45]). From the fitting in Fig. 4(b) (solid lines) by Eq. (3), when

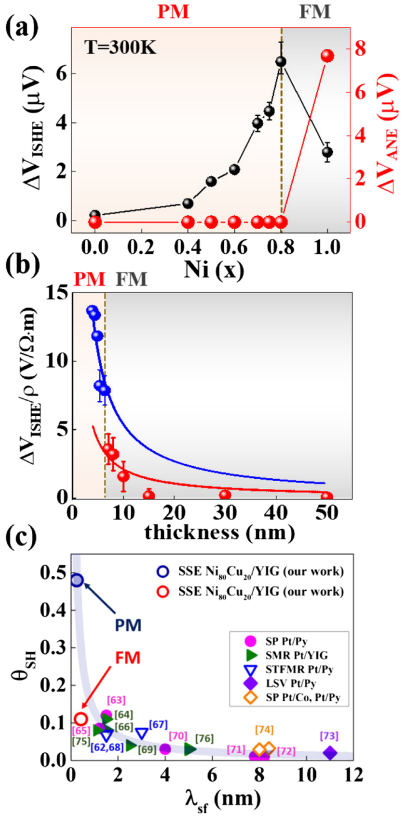

FIG. 4. (a) Composition dependence of ΔV_{ANE} for $Ni_xCu_{1-x}(5)$/Si and that of ΔV_{ISHE} for $Ni_xCu_{1-x}(5)$/YIG with $0 < x < 1.0$ at room temperature. (b) Thickness dependence of $\Delta V_{ISHE}/\rho$ (blue and red circles) and that of ΔV_{ANE} (purple circles) for $Ni_{80}Cu_{20}$; the blue and red solid curve are the fitted results using Eq. (3) for $Ni_{80}Cu_{20}$ in FM and PM state, respectively. (c) Plot of θ_{SH} versus λ_{sf} at room temperature. The blue and red open circles are the result for $Ni_{80}Cu_{20}$ in the PM and FM states. Other solid symbols are results for Pt in literature denoted by the references numbers,where the SP is spin pumping, SMR is spin Hall magnetoresistance, STFMR is spin-torque ferromagnetic resonance, and LSV is lateral spin valve. The blue curve represents $\theta_{SH}\lambda_{sf} = 0.13$ nm.

$Ni_{80}Cu_{20}$ is in the FM state ($t > 7$ nm), we obtain $\theta_{SH} = 11 \pm 2\%$ and $\lambda_{sf} = 0.42 \pm 0.08$ nm, which are comparable to the largest θ_{SH} of the heavy metals. On the other hand, when $Ni_{80}Cu_{20}$ is in the PM state ($t < 7$ nm), we obtain an even larger value of $\theta_{SH} = 46 \pm 9\%$ and $\lambda_{sf} = 0.22 \pm 0.04$ nm. Under the definition of θ_{SH} using number of carriers ($\theta_{SH} \le 1$), $\theta_{SH} = 38 \pm 8\%$ is the largest reported to date. The large spin conversion is further corroborated by the current-induced spin-orbit torque generated by $Ni_{80}Cu_{20}$ that shows high dampinglike torque efficiency of 0.4 and spin Hall angle of 0.5 (see Supplemental Material [45]).

Recent theoretical works have reported the enhancement of spin Hall conductivity σ_{SH} near the magnetic phase transition, where they attribute the mechanism to the coupling between conduction electron and dynamically

fluctuating local magnetic moment, which includes an optimistically estimated side-jump contribution of about $\sim 10^3\ \Omega^{-1}\,\mathrm{m}^{-1}$ and skew-scattering contribution of about $\sim 10^5\ \Omega^{-1}\,\mathrm{m}^{-1}$ [58]. We roughly estimate the σ_{SH} of $Ni_{80}Cu_{20}$ to be $\sim 8 \times 10^5\ \Omega^{-1}\,\mathrm{m}^{-1}$ by $\sigma_{SH} = \theta_{SH}/\rho$, which suggests the enhancement of θ_{SH} for $Ni_{80}Cu_{20}$ at T_C is dominated by the skew scatterings. Note that the spin-current injection efficiency C could also be enhanced during the magnetic instability [59–61]. Therefore, we include this contribution in the uncertainty.

Although θ_{SH} may vary significantly depending on the experimental technique or the analyses (e.g., Pt), empirically the relation of $\theta_{SH}\lambda_{sf} \approx$ const has been suggested as shown in Fig. 4(c) containing the results of various reports [62–76]]. Our results follow closely the correlation of $\theta_{SH}\lambda_{sf} \sim 0.13$ nm denoted as the blue curve. We attribute the enhanced spin-to-charge conversion and the larger θ_{SH} in $Ni_{80}Cu_{20}$ to enhanced electron skew scatterings during spin fluctuation that leads to the shorter λ_{sf}. Ni-Cu alloys in general, and $Ni_{80}Cu_{20}$ in particular, exhibit much larger spin-to-charge efficiency than those of Pt. Together with greatly reduced costs than precious metals, Ni-Cu alloys have a great potential for application in the fields of spintronics.

In summary, we study in the Ni-Cu alloys the interplay among the anomalous Nernst effect of the spin-polarized current, the inverse spin Hall effect of the pure spin current, and spin fluctuations, with tailored magnetic ordering temperature. We show that the spin-dependent thermal transport via the ANE can serve as a sensitive magnetometer to electrically detect magnetic phase transitions of thin films. Most importantly, we exploit the strong interaction of pure spin current and spin fluctuation to greatly enhance spin-to-charge conversion, yielding remarkably high spin Hall angle of 46% in $Ni_{80}Cu_{20}$ at room temperature, that can be exploited in various spin-based applications and devices.

The authors would like to thank S. Peng, X. Xu, and Y. Li from Johns Hopkins University and C. C. Chiang from National Taiwan University for experimental support. Work at Johns Hopkins University was supported by U.S. Department of Energy, Basic Energy Science Award No. DE-SC0009390. This work was supported by the Ministry of Science and Technology of Taiwan under Grant No. MOST 109-2123-M-002-002, No. MOST 110-2123-M-002-008, and No. MOST 110-2112-M-002-047-MY3. This study was also partially supported by Center of Atomic Initiative for New Materials by the Ministry of Education in Taiwan.

*danru@ntu.edu.tw
†clchien@jhu.edu
‡syhuang@phys.ntu.edu.tw

[1] M. N. Baibich, J. M. Broto, A. Fert, F. Nguyen Van Dau, F. Petroff, P. Etienne, G. Creuzet, A. Friederich, and J. Chazelas, Phys. Rev. Lett. **61**, 2472 (1988).
[2] G. Binasch, P. Grünberg, F. Saurenbach, and W. Zinn, Phys. Rev. B **39**, 4828(R) (1989).
[3] J. C. Slonczewski, J. Magn. Magn. Mater. **159**, L1 (1996).
[4] L. Berger, Phys. Rev. B **54**, 9353 (1996).
[5] M. I. Dyakonov and V. I. Perel, Phys. Lett. A **35**, 459 (1971).
[6] J. E. Hirsch, Phys. Rev. Lett. **83**, 1834 (1999).
[7] J. Sinova, S. O. Valenzuela, J. Wunderlich, C. H. Back, and T. Jungwirth, Rev. Mod. Phys. **87**, 1213 (2015).
[8] K. Ando, S. Takahashi, K. Harii, K. Sasage, J. Ieda, S. Maekawa, and E. Saitoh, Phys. Rev. Lett. **101**, 036601 (2008).
[9] L. Liu, C. F. Pai, Y. Li, H. W. Tseng, D. C. Ralph, and R. A. Buhrman, Science **336**, 555 (2012).
[10] A. Manchon, J. Železný, I. M. Miron, T. Jungwirth, J. Sinova, A. Thiaville, K. Garello, and P. Gambardella, Rev. Mod. Phys. **91**, 035004 (2019).
[11] Y. K. Kato, R. C. Myers, A. C. Gossard, and D. D. Awschalom, Science **306**, 1910 (2004).
[12] K. Ando and E. Saitoh, Nat. Commun. **3**, 629 (2012).
[13] H. L. Wang, C. H. Du, Y. Pu, R. Adur, P. C. Hammel, and F. Y. Yang, Phys. Rev. Lett. **112**, 197201 (2014).
[14] D. Qu, S. Y. Huang, B. F. Miao, S. X. Huang, and C. L. Chien, Phys. Rev. B **89**, 140407(R) (2014).
[15] D. Qu, S. Y. Huang, G. Y. Guo, and C. L. Chien, Phys. Rev. B **97**, 024402 (2018).
[16] N. H. D. Khang , Y. Ueda, and P. N. Hai , Nat. Mater. **17**, 808 (2018).
[17] D. Qu, T. Higo, T. Nishikawa, K. Matsumoto, K. Kondou, D. Nishio-Hamane, R. Ishii, P. K. Muduli, Y. Otani, and S. Nakatsuji, Phys. Rev. Mater. **2**, 102001(R) (2018).
[18] B. Zhao, D. Khokhriakov, Y. Zhang, H. Fu, B. Karpiak, A. M. Hoque, X. Xu, Y. Jiang, B. Yan, and S. P. Dash, Phys. Rev. Research **2**, 013286 (2020).
[19] M. Tian, Y. Zhu, M. Jalali, W. Jiang, J. Liang, Z. Huang, Q. Chen, Z. Zeng, and Y. Zhai, Front. Nanotechnol. **3**, 732916 (2021).
[20] B. F. Miao, S. Y. Huang, D. Qu, and C. L. Chien, Phys. Rev. Lett. **111**, 066602 (2013).
[21] C. Du, H. Wang, F. Yang, and P. C. Hammel, Phys. Rev. B **90**, 140407(R) (2014).
[22] D. Qu, S. Y. Huang, and C. L. Chien, Phys. Rev. B **92**, 020418(R) (2015).
[23] D. Tian, Y. Li, D. Qu, S. Y. Huang, X. Jin, and C. L. Chien, Phys. Rev. B **94**, 020403(R) (2016).
[24] T. C. Chuang, C. F. Pai, and S. Y. Huang, Phys. Rev. Applied **11**, 061005(R) (2019).
[25] T. C. Chuang, D. Qu, S. Y. Huang, and S. F. Lee, Phys. Rev. Research **2**, 032053(R) (2020).
[26] S. Y. Huang, D. Qu, T. C. Chuang, C. C. Chiang, W. Lin, and C. L. Chien, Appl. Phys. Lett. **117**, 190501 (2020).
[27] H. Wang, C. Du, P. C. Hammel, and F. Yang, Phys. Rev. Lett. **113**, 097202 (2014).
[28] W. Lin, K. Chen, S. Zhang, and C. L. Chien, Phys. Rev. Lett. **116**, 186601 (2016).
[29] Z. Qiu, J. Li, D. Hou, E. Arenholz, A. T. N' Diaye, A. Tan, K.-i. Uchida, K. Sato, S. Okamoto, Y. Tserkovnyak, Z. Q. Qiu, and E. Saitoh, Nat. Commun. **7**, 12670 (2016).
[30] L. Frangou, S. Oyarzún, S. Auffret, L. Vila, S. Gambarelli, and V. Baltz, Phys. Rev. Lett. **116**, 077203 (2016).

[31] J. Cramer, U. Ritzmann, B.-W. Dong, S. Jaiswal1, Z. Qiu, E. Saitoh, U. Nowak, and M. Kläui, J. Phys. D **51**, 144004 (2018).

[32] D. H. Wei, Y. Niimi, B. Gu, T. Ziman, S. Maekawa, and Y. Otani, Nat. Commun. **3**, 1058 (2012).

[33] Y. Ou, D. C. Ralph, and R. A. Buhrman, Phys. Rev. Lett. **120**, 097203 (2018).

[34] S. A. Ahern, M. J. C. Martin, and W. Sucksmith, Proc. R. Soc. B **248**, 145 (1958).

[35] M. W. Keller, K. S. Gerace, M. Arora, E. K. Delczeg-Czirjak, J. M. Shaw, and T. J. Silva, Phys. Rev. B **99**, 214411 (2019).

[36] N. Nagaosa, J. Sinova, S. Onoda, A. H. MacDonald, and N. P. Ong, Rev. Mod. Phys. **82**, 1539 (2010).

[37] S. O. Valenzuela and M. Tinkham, Nature (London) **442**, 176 (2006).

[38] T. C. Chuang, P. L. Su, P. H. Wu, and S. Y. Huang, Phys. Rev. B **96**, 174406 (2017).

[39] K. Uchida, H. Adachi, T. Ota, H. Nakayama, S. Maekawa, and E. Saitoh, Appl. Phys. Lett. **97**, 172505 (2010).

[40] E. Saitoh, M. Ueda, H. Miyajima, and G. Tatara, Appl. Phys. Lett. **88**, 182509 (2006).

[41] M. Harder, Y. S. Gui, and C. M. Hu, Phys. Rep. **661**, 1 (2016).

[42] R. Iguchi and E. Saitoh, J. Phys. Soc. Jpn. **86**, 011003 (2017).

[43] L. Vegard, Z. Phys. **5**, 17 (1921).

[44] A. R. Denton and N. W. Ashcroft, Phys. Rev. A **43**, 3161 (1991).

[45] See Supplemental Material at http://link.aps.org/supplemental/10.1103/PhysRevLett.128.227203 for magnetic properties, reproducibility of spin-dependent thermal measurement, spin injection coefficient C, thickness dependence of anomalous Nernst effect, current-induced spin-orbit torque magnetization switching, resistivity of Ni_xCu_{1-x} alloys, and discussion on the spin-current enhancement during spin fluctuation in 3d AFM materials, which includes Refs. [27–31, 46–53].

[46] A. Sola, P. Bougiatioti, M. Kuepferling, D. Meier, G. Reiss, M. Pasquale, T. Kuschel, and V. Basso, Sci. Rep. **7**, 46752 (2017).

[47] S. M. Wu, F. Y. Fradin, J. Hoffman, A. Hoffmann, and A. Bhattacharya, J. Appl. Phys. **117**, 17C509 (2015).

[48] S. M. Wu, W. Zhang, Amit KC, P. Borisov, J. E. Pearson, J. S. Jiang, D. Lederman, A. Hoffmann, and A. Bhattacharya, Phys. Rev. Lett. **116**, 097204 (2016).

[49] S. M. Rezende, R. L. Rodríguez-Suárez, R. O. Cunha, A. R. Rodrigues, F. L. A. Machado, G. A. Fonseca Guerra, J. C. Lopez Ortiz, and A. Azevedo, Phys. Rev. B **89**, 014416 (2014).

[50] C. Du, H. Wang, F. Yang, and P. C. Hammel, Phys. Rev. B **90**, 140407(R) (2014).

[51] K.-S. Lee, S.-W. Lee, B.-C. Min, and K.-J. Lee, Appl. Phys. Lett. **102**, 112410 (2013).

[52] Y. Deng, M. Yang, Y. Ji, and K. Wang, J. Magn. Magn. Mater. **496**, 165920 (2020).

[53] R. G. Delatorre, M. L. Sartorelli, A. Q. Schervenski, and A. A. Pasa, J. Appl. Phys. **93**, 6154 (2003).

[54] P. H. Wu, Y. T. Chan, T. C. Hung, Y. H. Zhang, D. Qu, T. M. Chuang, C. L. Chien, and S. Y. Huang, Phys. Rev. B **102**, 174426 (2020).

[55] E.-J. Guo, J. Cramer, A. Kehlberger, C. A. Ferguson, D. A. MacLaren, G. Jakob, and M. Kläui, Phys. Rev. X **6**, 031012 (2016).

[56] P. H. Wu, Y. C. Tu, D. Qu, H. L. Liang, S. F. Lee, and S. Y. Huang, Phys. Rev. B **101**, 104413 (2020).

[57] S. Varotto, M. Cosset-Chéneau, C. Grèzes, Y. Fu, P. Warin, A. Brenac, J. F. Jacquot, S. Gambarelli, C. Rinaldi, V. Baltz, J. P. Attané, L. Vila, and P. Noël, Phys. Rev. Lett. **125**, 267204 (2020).

[58] S. Okamoto, T. Egami, and N. Nagaosa, Phys. Rev. Lett. **123**, 196603 (2019).

[59] Y. Ohnuma, H. Adachi, E. Saitoh, and S. Maekawa, Phys. Rev. B **87**, 014423 (2013).

[60] L. Frangou, S. Oyarzún, S. Auffret, L. Vila, S. Gambarelli, and V. Baltz, Phys. Rev. Lett. **116**, 077203 (2016).

[61] B. Khodadadi, J. B. Mohammadi, C. Mewes, T. Mewes, M. Manno, C. Leighton, and C. W. Miller, Phys. Rev. B **96**, 054436 (2017).

[62] Y. Wang, P. Deorani, X. Qiu, J. H. Kwon, and H. Yang, Appl. Phys. Lett. **105**, 152412 (2014).

[63] M. Obstbaum, M. Hartinger, H. G. Bauer, T. Meier, F. Swientek, C. H. Back, and G. Woltersdorf, Phys. Rev. B **89**, 060407(R) (2014).

[64] M. Althammer *et al.*, Phys. Rev. B **87**, 224401 (2013).

[65] W. Zhang, V. Vlaminck, J. E. Pearson, R. Divan, S. D. Bader, and A. Hoffmann, Appl. Phys. Lett. **103**, 242414 (2013).

[66] N. Vlietstra, J. Shan, V. Castel, B. J. van Wees, and J. Ben Youssef, Phys. Rev. **B87**, 184421 (2013).

[67] L. Q. Liu, T. Moriyama, D. C. Ralph, and R. A. Buhrman, Phys. Rev. Lett. **106**, 036601 (2011).

[68] L. Q. Liu, R. A. Buhrman, and D. C. Ralph, arXiv: 1111.3702.

[69] H. Nakayama, M. Althammer, Y. T. Chen, K. Uchida, Y. Kajiwara, D. Kikuchi, T. Ohtani, S. Geprägs, M. Opel, S. Takahashi, R. Gross, G. E. W. Bauer, S. T. B. Goennenwein, and E. Saitoh, Phys. Rev. Lett. **110**, 206601 (2013).

[70] V. Vlaminck, J. E. Pearson, S. D. Bader, and A. Hoffmann, Phys. Rev. B **88**, 064414 (2013).

[71] H. Nakayama, K. Ando, K. Harii, T. Yoshino, R. Takahashi, Y. Kajiwara, K. Uchida, Y. Fujikawa, and E. Saitoh, Phys. Rev. B **85**, 144408 (2012).

[72] Z. Feng, J. Hu, L. Sun, B. You, D. Wu, J. Du, W. Zhang, A. Hu, Y. Yang, D. M. Tang, B. S. Zhang, and H. F. Ding, Phys. Rev. B **85**, 214423 (2012).

[73] M. Morota, Y. Niimi, K. Ohnishi, D. H. Wei, T. Tanaka, H. Kontani, T. Kimura, and Y. Otani, Phys. Rev. B **83**, 174405 (2011).

[74] X. Tao, Q. Liu, B. Miao, R. Yu, Z. Feng, L. Sun, B. You, J. Du, K. Chen, S. Zhang, L. Zhang, Z. Yuan, D. Wu, and H. Ding, Sci. Adv. **4**, eaat 1670 (2018).

[75] N. Vlietstra, J. Shan, V. Castel, J. Ben Youssef, G. E. W. Bauer, and B. J. van Wees, Appl. Phys. Lett. **103**, 032401 (2013).

[76] C. Hahn, G. de Loubens, O. Klein, M. Viret, V. V. Naletov, and J. Ben Youssef, Phys. Rev. B **87**, 174417 (2013).